Dalton Transactions

PAPER

View Article Online
View Journal | View Issue

Cite this: *Dalton Trans.*, 2019, **48**, 17908

The first coordination polymers with an $[O]_2[N]P(S)$-Hg segment: a combined experimental, theoretical and database study†

Elham Torabi Farkhani,[a] Mehrdad Pourayoubi, *[a] Mohammad Izadyar,[a] Pavel V. Andreev[b] and Ekaterina S. Shchegravina[c]

Received 2nd September 2019,
Accepted 11th November 2019

DOI: 10.1039/c9dt03546j

rsc.li/dalton

The study of one-dimensional coordination polymers $\{Hg_2Cl_4L_1\}_n$ (**1**), $\{HgBr_2L_1\}_n$ (**2**) and $\{Hg_2Cl_4L_2\}_n$ (**3**) (L_1 = $(S)P(OC_2H_5)_2NHC_6H_4NHP(S)(OC_2H_5)_2$ and L_2 = $(S)P(OC_2H_5)_2NC_4H_8NP(S)(OC_2H_5)_2$) is the first such structural study of Hg(II) coordination polymers with $(O)_2(N)PS$-based ligands. The mercury atoms adopt a distorted trigonal pyramidal environment, $Hg(Cl)_3(S)$ for **1** and **3** and $Hg(Br)_2(S)_2$ for **2**, and the difference observed in the stoichiometry of mercury halide to the thiophosphoramide ligand in **1** and **3** with respect to the one in **2** is a result of the formation of the Hg_2Cl_2 ring, however, the molar ratio 2 : 1 of HgX_2 (X = Cl and Br) to ligand was used for the preparation of all three complexes. The strengths of mercury-sulfur and mercury-halide covalent bonds are evaluated by theoretical calculations (QTAIM and NBO) which show their principally electrostatic nature with a partial covalent contribution. The energies of interactions building supramolecular assemblies and intramolecular interactions, *i.e.* NH···Cl, NH···Br, CH···Cl, CH···Br, CH···O, CH···S and CH···π, are theoretically evaluated. The characteristic structural features arising from the aromatic/aliphatic linkers in the ligands and chloride/bromide attached to mercury are investigated by Hirshfeld surface analysis and fingerprint plots.

Introduction

Crystal engineering of coordination polymers is a multidisciplinary field with potential technological applications.[1] In this domain, knowledge about metal–ligand coordination bond strength, frequently observed coordination geometries associated with metal ions and directionality helps in constructing diverse supramolecular architectures from the organization of structural building blocks.[2] Thus, it is possible to design and synthesize targeted one-, two- or three-dimensional coordination polymers by carefully choosing ligands and metal precursors.[3,4] However, the structural features are also related to the flexible coordination environment of a metal ion, ligand flexibility, number of donor sites in the ligand, metal to ligand ratio and reaction conditions.[5]

A variety of metal complexes were prepared, and their structures and physicochemical properties were studied.[6,7] Among them, mercury with a d^{10} electronic configuration presents a flexible coordination environment with a variety of coordination numbers from as low as two[8] and three[9] to higher, four[10] up to eight,[11] nine[12] and ten[13] and it can adopt a wide range of coordination geometries, with linear, trigonal planar and tetrahedral being the most common.[14] The formation of polymers with mercury(II) seems to be surprisingly sparse, and, despite the attractive properties of mercury(II) compounds in terms of their different applications[15] (although somewhat limited due to mercury's toxicity), there have been only very few reports on Hg(II) polymers with sulfur donor-based ligands to date.[16,17]

For metal complexes with $[O]_2[N]P(S)$-based ligands, a search on the Cambridge Structural Database (CSD, version 5.40, updated to November 2018[18]) yielded 76 structures featuring sulfur coordinated to metal cations, which include seventeen different elements (s-/p-block: Na, K, Sr, and Pb; d-block: Cu, Co, Fe, Ni, Re, Zn, Cd, Ru, Ag, Au, Pt, Pd, and Te), typically, structures with the CSD refcodes BAXSAV,[19] IMAMAL,[20] REHGES01[21] and TEQHOO,[22] with none of them being mercury (Fig. S1†). Some of these structures include an additional Lewis base site(s) in the ligand,[23–25] however, there is only one report of coordination polymers in this category of

[a]*Department of Chemistry, Faculty of Science, Ferdowsi University of Mashhad, Mashhad, Iran. E-mail: pourayoubi@um.ac.ir*
[b]*Department of Physics, N. I. Lobachevsky State University of Nizhni Novgorod, pr. Gagarina, 23-3, Nizhni Novgorod, Russia*
[c]*Department of Chemistry, Lobachevsky State University of Nizhni Novgorod, Gagarin Avenue, 23, Nizhni Novgorod, Russia*

† Electronic supplementary information (ESI) available. CCDC 1056128, 1460892, and 1054208. For ESI and crystallographic data in CIF or other electronic format see DOI: 10.1039/C9DT03546J

ligands, in the case of silver(I), where a bidentate ligand including two P=S groups was used.[26]

In this article we investigate the formation of coordination polymers of mercury by using both aliphatic and aromatic spacers between two P=S groups in ligands, resulting in the following polymers: $\{Hg(Cl)(\mu\text{-}Cl)_2Hg(Cl)[(S)P(OC_2H_5)_2NHC_6H_4NHP(OC_2H_5)_2(S)]\}_n$ (**1**), $\{HgBr_2[(S)P(OC_2H_5)_2NHC_6H_4NHP(OC_2H_5)_2(S)]\}_n$ (**2**) and $\{Hg(Cl)(\mu\text{-}Cl)_2Hg(Cl)[(S)P(OC_2H_5)_2NC_4H_8NP(OC_2H_5)_2(S)]\}_n$ (**3**), which represent the first examples of coordination polymers with an $[O]_2[N]P(S)$-Hg segment. The compounds were studied by X-ray single-crystal diffraction, IR spectroscopy, and mass spectrometry, and also by solution $^{31}P\{^1H\}$, ^1H, $^{13}C\{^1H\}$ and ^1H–^{15}N (HSQC) NMR spectroscopy for two soluble compounds. DFT calculations are employed to evaluate the energies of coordination linkages and also of non-covalent interactions in the polymers, which allow their impact on the final structures to be addressed.

Experimental

Materials and general methods

All reagents used in this study were obtained from commercial sources and used as received. ^1H, ^{13}C, and ^{31}P NMR spectra were recorded on a Bruker Avance DRX 400 spectrometer. Chemical shifts were determined relative to internal TMS (tetramethylsilane) for ^1H and ^{13}C and relative to external 85% H_3PO_4 for ^{31}P. A ^1H–^{15}N HSQC experiment was carried out on an Agilent DDR2 400 spectrometer. IR spectra were recorded on a Buck 500 scientific spectrometer using KBr pellets. Elemental analyses (C, H and N) were performed using a Thermo Finnigan Flash 1112EA elemental analyzer. The mass spectra were recorded with an MS model 5973 Network Mass Selective Detector.

Synthesis

Synthesis of L_1 and L_2. The synthesis of ligand L_1 was performed according to the literature procedure[27] with a few modifications which are related to the nonusage of 4-dimethylaminopyridine and 1,2-ethylene diamine. The synthesis of L_1 was done by a reaction between *O*,*O*′-diethyl chlorothiophosphate (2 mmol, 0.377 g), 1,4-phenylenediamine (1 mmol, 0.108 g) and triethylamine (2 mmol, 0.202 g) in dry acetonitrile (15 ml) at 273 K. Ligand L_2 was prepared using a similar procedure as follows: a solution of piperazine (1 mmol, 0.086 g) and triethylamine (2 mmol, 0.202 g) in dry acetonitrile (10 ml) was added dropwise to a stirred solution of *O*,*O*′-diethyl chlorothiophosphate (2 mmol, 0.377 g) in the same solvent (15 ml) at 273 K. After 5 hours of stirring, the solvent was removed in a vacuum and the solid formed was washed with distilled water to remove triethylamine hydrochloride salt (Scheme 1).

L_1: $(C_2H_5O)_2P(S)(NHC_6H_4NH)P(S)(OC_2H_5)_2$

^1H and ^{13}C NMR spectra in $CDCl_3$, IR spectrum and X-ray crystallography data of L_1 were previously reported.[27] Here the data of ^{31}P and 2D ^1H–^{15}N HSQC NMR in CD_3CN are reported, besides, a re-investigation of ^1H and ^{13}C NMR (in CD_3CN). ^1H NMR (400 MHz, CD_3CN): δ = 1.26 (t, $^3J_{H-H}$ = 7.0 Hz, 12H), 4.08 (m, 8H), 6.21 (d, $^2J_{P-H}$ = 14.4 Hz, 2H), 6.99 (s, 4H). $^{13}C\{^1H\}$ NMR (101 MHz, CD_3CN): δ = 15.12 (d, $^3J_{P-C}$ = 8.2 Hz), 62.90 (d, $^2J_{P-C}$ = 4.5 Hz), 119.40 (d, $^3J_{P-C}$ = 6.7 Hz), 134.68 (d, $^2J_{P-C}$ = 3.1 Hz). $^{31}P\{^1H\}$ NMR (162 MHz, CD_3CN): δ = 65.42 (s). ^1H–^{15}N corr. (CD_3CN): {–294.93, 6.23}. Anal. calcd for $C_{14}H_{26}N_2O_4P_2S_2$ (%): C, 40.77; H, 6.35; N, 6.79. Found: C, 41.15; H, 6.35; N, 7.01. MS (70 eV, EI): *m*/*z* (%) = 412 (94) $[M]^+$, 411 (100) $[M-1]^+$, 152 (50) $[C_4H_9O_2PS]^+$, 124 (82) $[C_2H_5O_2PS]^+$, 106 (88) $[C_6H_6N_2]^+$, 28 (88) $[C_2H_4]^+$.

L_2: $(C_2H_5O)_2P(S)(NC_4H_8N)P(S)(OC_2H_5)_2$

IR (KBr, cm^{-1}): 2990, 2903, 2865, 1846, 1764, 1449, 1387, 1339, 1264, 1151, 1098, 1030, 972, 792, 714, 625. ^1H NMR (400 MHz, DMSO-d_6): δ = 1.21 (t, $^3J_{H-H}$ = 7.0 Hz, 12H), 3.10 (m, 8H), 3.91 (m, 8H). $^{13}C\{^1H\}$ NMR (101 MHz, DMSO-d_6): δ = 16.12 (d, $^3J_{P-C}$ = 8.1 Hz), 45.33 (d, $^2J_{P-C}$ = 8.1 Hz), 62.87 (d, $^2J_{P-C}$ = 5.3 Hz). $^{31}P\{^1H\}$ NMR (162 MHz, DMSO-d_6): δ = 73.64 (s). Anal. calcd for $C_{12}H_{28}N_2O_4P_2S_2$ (%): C, 36.91; H, 7.23; N, 7.17. Found: C, 37.81; H, 7.16; N, 7.26. MS (70 eV, EI): *m*/*z* (%) = 390 (27) $[M]^+$, 153 (100) $[C_4H_{10}O_2PS]^+$, 124 (29) $[C_2H_5O_2PS]^+$, 84 (99) $[C_4H_8N_2]^+$, 28 (66) $[C_2H_4]^+$.

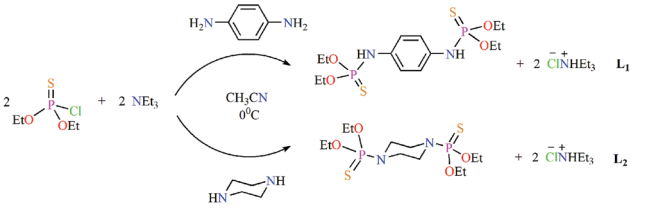

Scheme 1 Preparation of L_1 and L_2.

Synthesis of complexes

For the preparation of complexes, a solution of $HgCl_2$ (2 mmol, 0.543 g) or $HgBr_2$ (2 mmol, 0.721 g) in 15 ml methanol was added dropwise to a solution of the corresponding ligand (1 mmol, 0.412 g (L_1) or 0.390 g (L_2)) in the same solvent (10 ml). The clear solution was stirred under reflux for 24 hours. Crystals suitable for X-ray diffraction were obtained from slow evaporation of the solvent at room temperature. The chemical structures of the complexes are represented in Scheme 2.

1: $\{Hg(Cl)(\mu\text{-}Cl)_2Hg(Cl)[(S)P(OC_2H_5)_2(NHC_6H_4NH)P(S)(OC_2H_5)_2]\}_n$. IR (KBr, cm^{-1}): 3209, 2988, 1612, 1513, 1479, 1380, 1342, 1275, 1220, 1164, 1104, 990, 957, 828, 797, 727, 634. ^1H NMR (400 MHz, CD_3CN): δ = 1.27 (t, $^3J_{H-H}$ = 7.0 Hz, 12H), 4.10 (m, 8H), 6.28 (d, $^2J_{P-H}$ = 14.4 Hz, 2H), 7.00 (s, 4H). $^{13}C\{^1H\}$ NMR (101 MHz, CD_3CN): δ = 15.09 (d, $^3J_{P-C}$ = 8.3 Hz), 63.12 (d, $^2J_{P-C}$ = 4.7 Hz), 119.48 (d, $^3J_{P-C}$ = 6.6 Hz). $^{31}P\{^1H\}$ NMR (162 MHz, CD_3CN): δ = 65.09 (s). ^1H–^{15}N corr. (CD_3CN): {–298.20, 6.25}. Anal. calcd for $C_{14}H_{26}Cl_4Hg_2N_2O_4P_2S_2$ (%): C, 17.60; H, 2.74; N, 2.93. Found: C, 17.85; H, 2.69; N, 2.93. MS (20 eV, EI): *m*/*z* (%) = 684 (6) $[^{35}Cl_2{}^{202}HgL_1]^+$, 411 (8) $[L_1-1]^+$, 79

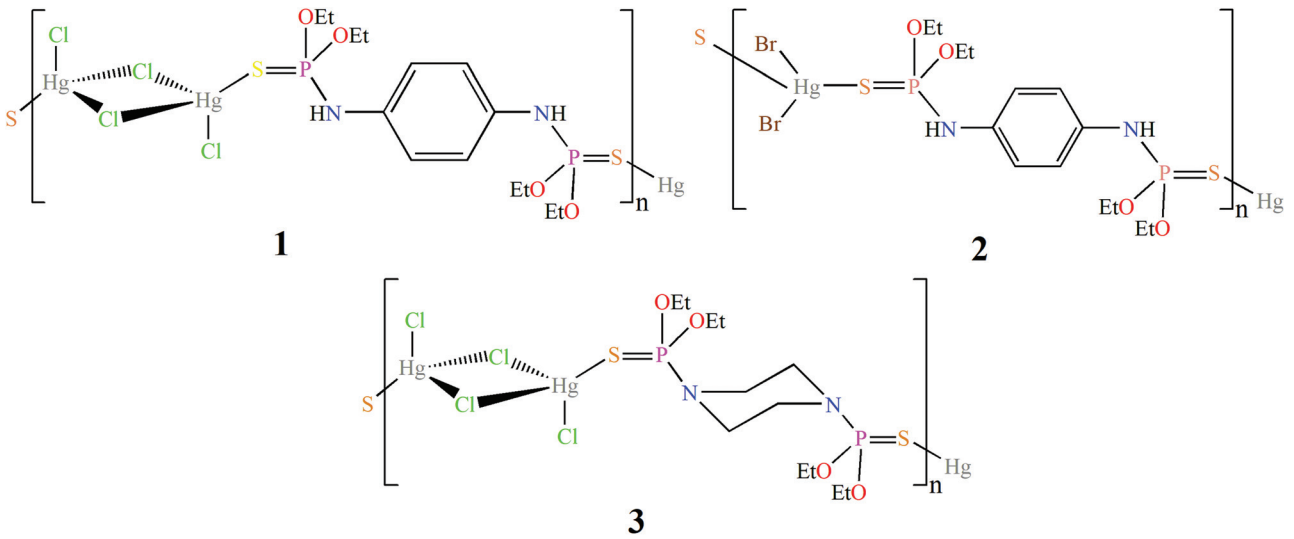

Scheme 2 Schematic representation of the complexes.

(100) $[C_6H_7]^+$. MS (70 eV, EI): *m*/*z* (%) = 648 (<1) $[^{35}Cl_2{}^{202}HgL_1-H^{35}Cl]^+$, 43 (100) $[C_2H_3O]^+$.

2: $\{HgBr_2[(S)P(OC_2H_5)_2(NHC_6H_4NH)P(S)(OC_2H_5)_2]\}_n$. IR (KBr, cm^{-1}): 3267, 2986, 1742, 1565, 1515, 1477, 1380, 1277, 1217, 1165, 1096, 1022, 967, 821, 729, 649. MS (20 eV, EI): *m*/*z* (%) = 772 (<1) $[^{79}Br_2{}^{202}HgL_1]^+$, 412 (100) $[L_1]^+$. MS (70 eV, EI): *m*/*z* (%) = 772 (<1) $[^{79}Br_2{}^{202}HgL_1]^+$, 412 (57) $[L_1]^+$, 97 (100) $[H_3O_2PS]^+$.

3: $\{Hg(Cl)(\mu\text{-}Cl)_2Hg(Cl)[(S)P(OC_2H_5)_2(NC_4H_8N)P(S)(OC_2H_5)_2]\}_n$. IR (KBr, cm^{-1}): 2976, 2896, 1776, 1614, 1445, 1384, 1344, 1298, 1266, 1122, 1038, 968, 897, 804, 772, 702. ^{1}H NMR (400 MHz, DMSO-d_6): δ = 1.24 (t, $^3J_{H-H}$ = 9.4 Hz, 12H), 3.13 (t, $^3J_{H-H}$ = 11.6 Hz, 8H), 3.90–4.00 (m, 8H). $^{13}C\{^1H\}$ NMR (101 MHz, DMSO-d_6): δ = 16.14 (d, $^3J_{P-C}$ = 10.7 Hz), 45.30 (d, $^2J_{P-C}$ = 9.4 Hz), 63.01 (d, $^2J_{P-C}$ = 7.4 Hz). $^{31}P\{^1H\}$ NMR (162 MHz, DMSO-d_6): δ = 73.34. Anal. calcd for $C_{12}H_{28}Cl_4Hg_2N_2O_4P_2S_2$ (%): C, 15.44; H, 3.02; N, 3.00. Found: C, 15.67; H, 2.91; N, 2.99. MS (20 eV, EI): *m*/*z* (%) = 662 (<1) $[^{35}Cl_2{}^{202}HgL_2]^+$, 169 (100) $[C_4H_{12}NO_2PS]^+$. MS (70 eV, EI): *m*/*z* (%) = 663 (<1) $[^{35}Cl_2{}^{202}HgL_2 + 1]^+$, 169 (100) $[C_4H_{12}NO_2PS]^+$.

X-ray crystallography

The diffraction data were collected using an Xcalibur, Sapphire3, Gemini (293 K and λ = 0.71073 Å) X-ray diffractometer and the data were processed with the CrysAlisPro[28] program. The positions of all non-hydrogen atoms were refined on F^2 by a full-matrix least-squares procedure with the SHELXL2014/7.[29,30] All carbon-bound hydrogen atoms were located geometrically (C–H = 0.95–1.00 Å) and refined using a riding model with the $U_{iso}(H) = 1.2U_{eq}(C)$ ($1.5U_{eq}(C)$ for methyl groups). For **1** and **2**, the hydrogen atoms connected to the nitrogen atoms were located in electron density difference maps and refined without constraints and restraints. Crystal data, data collection and refinement details are summarized in Table S1† and selected bond lengths and angles are given in Table S2.† Crystal structure visualization was obtained using OlexSys.[31] Further details are available from the Cambridge Crystallographic Data Centre through CCDC numbers 1056128 (**1**), 1460892 (**2**) and 1054208 (**3**).†

Theoretical methods

Density functional theory (DFT) calculations were performed using the GAUSSIAN09 package.[32] All calculations were carried out by using the M06-2X functional,[33] the LANL2DZ[34] basis set for Hg and Br and the 6-311++G(d,p) basis set for other atoms without any symmetry restriction. To gain an insight into the electronic charge transfer processes, natural bond orbital (NBO) analysis was applied.[35] In order to describe the topological properties at the bond critical points (BCPs), the quantum theory of atoms-in-molecules (QTAIM)[36] procedure was followed at the same level of theory, using the MultiWFN program,[37] with a wave function generated by the Gaussian program.

Hirshfeld surface analysis

Hirshfeld surface (HS)[38] and 2D fingerprint (FP) plot[39] analyses can be considered as fundamental methods for the exploration of intermolecular contacts in supramolecular structures.[40,41] Each point on the HS has a well-defined distance from the nearest atom inside the surface (d_i), and analogously, a distance from the nearest atom outside the surface (d_e). The mathematical treatment of d_e and d_i values with selected functions (*i.e.* d_{norm}, shape index, and curvedness) allows particular structural information (typically π–π stacking and hydrogen bonding) to be highlighted using the color mapping of the HS. In the case of the d_{norm} function, red spots are associated with the contacts between atoms on both sides of the HS, which have a distance smaller than the sum of van der Waals radii, and for this reason, d_{norm} representations are frequently used to visualize short contacts, *e.g.* hydrogen bonds. In addition, plotting the histogram of all (d_e, d_i) contacts gives a two-dimensional (2D) fingerprint plot, which can

be treated as a graphical 'summary' of the contact distances to the HS; consequently, their shapes are diagnostic for given intermolecular contacts. The HSs, mapped with the d_{norm} functions, and 2D FPs of compounds **1**, **2** and **3** were generated using the Crystal Explorer package ver. 3.1[42] with the CIF files of crystal structures as the input files.

Results and discussion

Structure description

In the synthesis procedure of coordination polymers, the molar ratio 2 : 1 of HgX_2 (X = Cl and Br) to ligand was used, and both two polymers with chlorido ligands (**1** and **3**) show the same stoichiometry of $HgCl_2$: ligand (2 : 1); however the polymer with bromido (**2**) shows a lower contribution of $HgBr_2$ with a stoichiometry of 1 : 1 for metal to ligand.

Fig. S2† presents the asymmetric units of **1**, **2** and **3**. For each of **1** and **3**, the asymmetric unit consists of one-half of the structural unit (monomer), which includes one mercury, two chlorines, and one-half of the ligand, while the asymmetric unit of **2** is composed of two-half ligands and one $HgBr_2$ moiety. The whole monomers of all three structures are generated by an inversion element, which is located at the center of NHC_6H_4NH and NC_4H_8N bridges.

The structural units of **1**, **2** and **3** are given in Fig. 1. In these structures, the thiophosphoramide ligands are coordinated to mercury through σ-donor sulfur atoms, and the P═S groups are on two different sides with respect to the bridge segments. The P═S bond lengths in **1** (1.9765(10) Å) and **2** (1.9688(17) and 1.9694(14) Å) are slightly longer than that of the free ligand (1.9320(15) Å),[27] and the P═S bond length in **3** (1.986(3) Å) is not so different.

The best overlays of complexes **1** and **2** with the corresponding ligand L_1 are shown in Fig. S3† (top and bottom). The overlay of **1**/L_1 shows large torsional liberty at the positions of ethyl chains. The bulky mercury-containing fragment of **1** pushes the neighbor ethyl group towards the phenyl ring and the neighborhood of ethyl and phenyl groups leads to an intramolecular C–H···π interaction which will be discussed later. Complex **2** shows a better similarity with L_1, compared to that seen for complex **1**.

In structures **1** and **3**, there are three different Hg–Cl bonds, related to the terminal and two bridging chlorido ligands. The bridging chlorido ligands act as a μ-linker to connect two Hg atoms creating a four-membered Hg_2Cl_2 ring, and each mercury(II) center is within an [S][Cl]Hg(μ-Cl)$_2$ environment. In this planar ring of structure **1**, a considerable difference of about 0.34 Å was found between the bond lengths of bridging chlorido ligand and two mercury atoms in two sides (two Hg1–Cl2 2.4864(8) Å and two Hg1–Cl2^{ii} 2.8276 (8) Å; symmetry code (ii) $-x + 3, -y + 2, -z + 2$), demonstrating different strengths of mercury-chlorine bonds in the ring. The $[Hg_2X_2]$ ring is a common structural motif in the mercury(II) halide complexes.[43,44] The bond lengths noted and the two other bond lengths received by each mercury atom (*i.e.* Hg1–S1 2.4444(8) Å, Hg1–Cl1 2.4290(9) Å in **1**) are within the expected ranges for analogous structures.[45,46] Typically, a summary of CSD survey on the Hg–S bond lengths, without any restriction, for all of the structures including this bond is given in Fig. 2. The dataset for this survey includes 1482 structures with 3407 Hg–S bond distances and the data vary within 2.12 to 3.40 Å with the maximum populations within 2.4 to 2.5 Å (935 hits, about 27%).

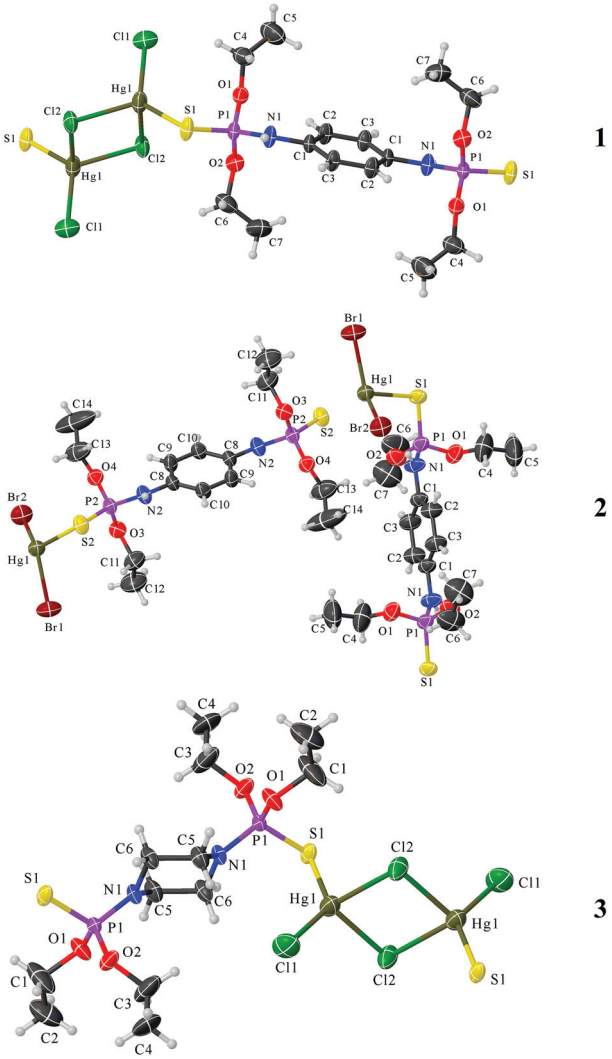

Fig. 1 Displacement ellipsoid plots (50% probability level) of the structural units.

There are some reports on the structures including the [S][Cl]Hg(μ-Cl)$_2$Hg[Cl][S] segment in the literature,[47–49] but there is no report of S atom belonging to an [O]$_2$[N]P(S)-based ligand, and we report the first X-ray crystal structures of complexes (and coordination polymers) in this family. For another family of thiophosphoramide ligands, with the (N)$_3$P(S) skeleton, there is only one report of a monomeric Hg complex.[50]

The geometry of four atoms/groups around a central atom can be described by an angular index $\tau_4 = [360 - (\alpha + \beta)]/141$, where α and β are the two largest angles around the four-co-

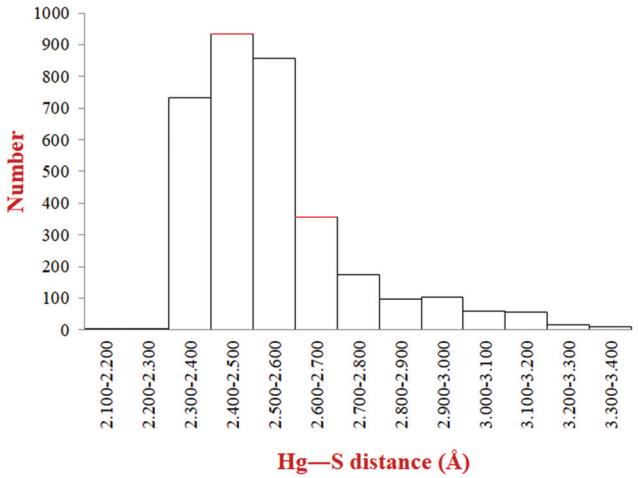

Fig. 2 Histogram of the Hg–S distances extracted from the crystal structures in the CSD, and the title structures. The Hg–S bond distances of the title structures are specified as red colors in the columns which belong to the same regions.

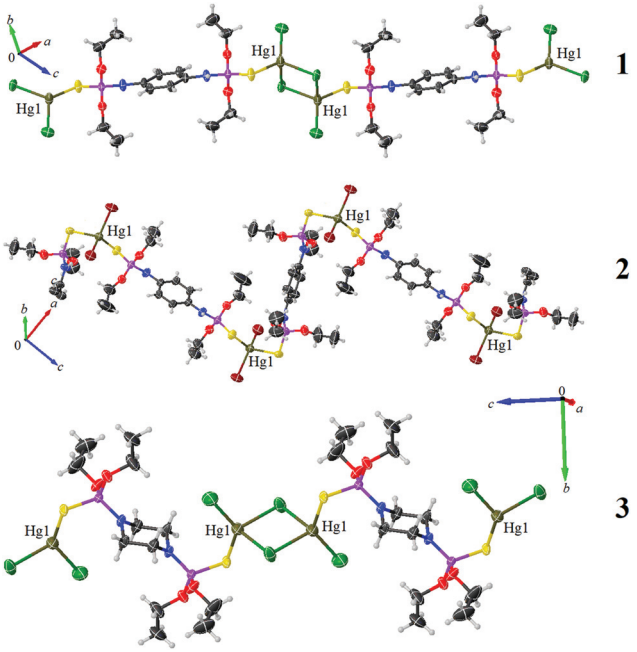

Fig. 3 Displacement ellipsoid plot (50% probability level) of a part of a one-dimensional chain in each of the coordination polymers **1**, **2** and **3**.

ordinate center, and the values of zero for square planar, 0.07, 0.18, 0.5 and 0.64 for seesaw (typically for θ = 90°, τ_4 is 0.64) and 0.85 and 1 for trigonal pyramidal and tetrahedral, respectively are obtained.[51] The angular indexes of 0.87, 0.86 and 0.84 were obtained for the mercury environments of **1**, **2** and **3**, respectively, describing a nearly trigonal pyramidal shape for three structures. In the typical structure **1**, the bond angles specifying this shape at the Hg(II) center are as follows: Cl1–Hg1–S1 125.46(4)°, Cl2–Hg1–S1 118.69(3)°, Cl1–Hg1–Cl2 111.08(4)°, $Cl2^{i}$–Hg1–S1 108.49(3)°, Cl1–Hg1–$Cl2^{i}$ 94.56(3)° and Cl2–Hg1–$Cl2^{i}$ 86.91(3)° (symmetry code: (i) $-x + 1, -y + 2, -z + 1$).

Fig. 3 presents a view of the coordination polymers **1**, **2** and **3**. In both structures **1** and **3**, the bridging chlorido ligands connect adjacent monomers to form a one-dimensional framework, along the [101] axis in structure **1** and parallel to the *c* axis, *i.e.* [001], in structure **3**.

In structure **2**, the Hg(II) center shows a four-coordinate $HgBr_2(S)(S)$ environment, with the Hg–S of 2.6625(13) and 2.6076(11) Å and the Hg–Br of 2.5338(5) and 2.5482(5) Å; thus, the coordination polymeric structure is constructed through the connection of $HgBr_2$ moieties by the bidentate ligands, in the [101] direction, which is different from structures **1** and **3**, in which the formation of the Hg_2Cl_2 ring leads to the construction of polymeric structures.

The Hg–S–P angles of **1**, **2** and **3** are 100.82(4)°, 96.76(5)°/102.38(6)° and 98.49(10)°, respectively. For comparison, the angles around the two-coordinated sulfur atoms in $(O)_2(N)P{=}S{-}M$ structures (M is metal) were analyzed for 76 structures retrieved from the CSD including 158 M–S–P bond angles and a summary of the analysis is shown in Fig. S4.† The data are spread within 76.8° to 119.1° with the maximum population in the range of 95° to 100° (59 hits of the total 158 hits, about 37%).

Fig. 4 presents the hydrogen bond patterns of **1** and **2**. In structure **1**, the adjacent linear coordination polymers are linked through intermolecular N1–H1···$Cl1^{iii}$ interactions (N···Cl^{iii} = 3.299(3) Å; symmetry code: (iii) $x + 1, y, z$, Table 1), building a two-dimensional supramolecular assembly parallel to the *ac* plane, and also include weak intramolecular C2–H2···O1 and C4–H4*A*···Cl1 interactions.

N1–H1···Br2 in **2** is an intramolecular interaction (H1···Br2 = 2.54 Å), and the three-dimensional supramolecular structure of **2** is constructed by C–H···Br hydrogen bonds (with H···Br distances of 2.99 Å for C4–H4*A*···$Br2^{iii}$, 2.90 Å for C13–H13*B*···$Br1^{iv}$ and 3.13 Å for C10–H10···$Br1^{v}$ (symmetry codes: (iii) $-x + 1, -y, -z + 1$; (iv) $x, y + 1, z$; (v) $-x, y + 1/2, -z + 1/2$, Table 1). In the structures **1** and **2**, the phenyl rings participate in C–H···π interactions (CH belongs to the ethyl group) [in **1**: intramolecular C7–H7*B*···Cg interaction, H7*B*···Cg = 3.49(1) Å (Fig. S5†) and in **2**: intramolecular C14–H14*A*···Cg (3.49 Å) and C14–H14*B*···Cg interactions (3.93 Å), Fig. S6†].

Structure **3** does not include N–H bonds and the supramolecular two-dimensional hydrogen-bonded assembly, parallel to the *bc* plane, is formed by the cooperation of intermolecular C4–H4*A*···$S1^{iii}$ and C4–H4*C*···$Cl1^{iv}$ hydrogen bonds (symmetry codes: (iii) $x, -y + 3/2, z + 1/2$; (iv) $-x, y + 1/2, -z + 1/2$, Fig. S7†). In this assembly, one intramolecular C–H···Cl interaction is also found.

Theoretical results and discussion

To evaluate the mercury-sulfur and mercury-halogen bond strengths, the LHg_2Cl_4L (L = L_1 and L_2) fragments for complexes **1** and **3** and the $HgBr_2(L_1)_2$ fragment for complex **2** were constructed from the X-ray crystal structures and used as input files for the chemical calculations. NBO and QTAIM analyses were performed for the fully optimized structures noted. For

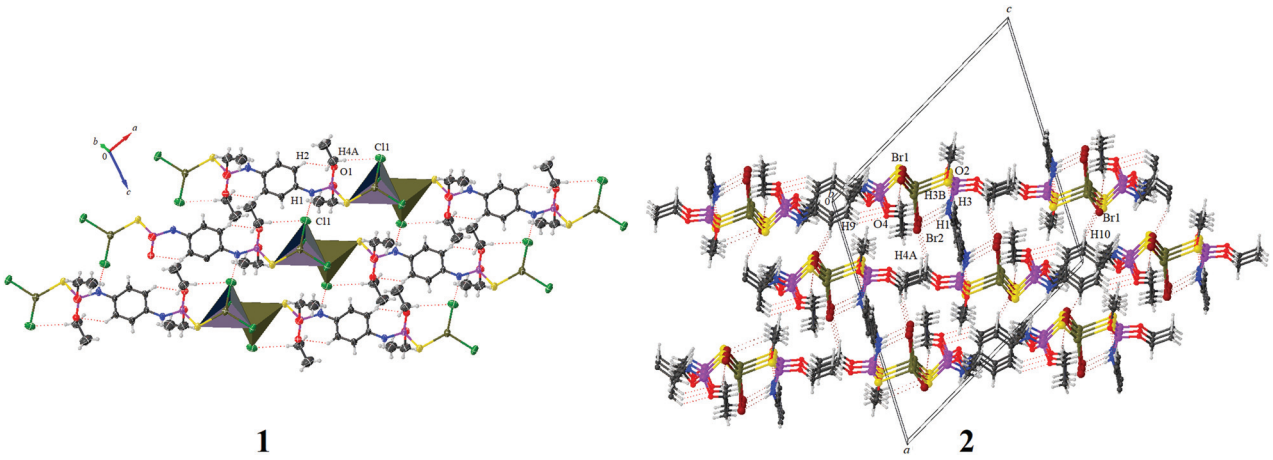

Fig. 4 Presentation of the hydrogen bond patterns of **1** and **2**.

Table 1 Hydrogen bonds for complexes (Å and °)

D–H···*A*	*D*–H	H···*A*	*D*···*A*	*D*–H···*A*
1				
N1–H1···Cl1^{iii}	0.85(2)	2.48(2)	3.299(3)	165(3)
C2–H2···O1	0.93	2.57	3.227(3)	128
C4–H4*A*···Cl1	0.97	2.80	3.654(5)	148
C7–H7*B*···Cg	0.96	3.49(1)	4.36(1)	152(1)
2				
C9–H9···O4	0.93	2.45	3.132(5)	130
C4–H4*B*···S1	0.97	2.93	3.419(7)	113
C4–H4*A*···Br2^{iii}	0.97	2.99	3.762(7)	138
N1–H1···Br2	0.86	2.54	3.398(4)	172
C3–H3···O2	0.93	2.49	3.142(6)	127
C11–H11*B*···S2	0.97	3.00	3.480(5)	112
C13–H13*B*···Br1^{iv}	0.97	2.90	3.829(7)	161
C10–H10···Br1^{v}	0.93	3.13	3.895(4)	141
C14–H14*A*···Cg	0.96	3.49	4.072(11)	121(4)
C14–H14*B*···Cg	0.96	3.93	4.072(11)	91(4)
3				
C4–H4*A*···S1^{iii}	0.96	2.99	3.902(8)	158
C4–H4*C*···Cl1^{iv}	0.96	2.92	3.870(11)	171
C5–H5*A*···Cl1	0.97	2.95	3.764(7)	142

Symmetry codes: **1**: (iii) $x+1, y, z$; **2**: (iii) $-x+1, -y, -z+1$; (iv) $x, y+1, z$; (v) $-x, y+1/2, -z+1/2$; **3**: (iii) $x, -y+3/2, z+1/2$; (iv) $-x, y+1/2, -z+1/2$.

comparison with the complexes, the ligands were theoretically studied and for L_1 the X-ray crystal structure was used as the input file.

The selected optimized geometrical parameters of complexes **1**, **2** and **3** are represented in Table S2.† As expected, the calculated P═S bond lengths in **1** (1.9864 Å), **2** (1.9731 and 1.9755 Å) and **3** (2.0026 Å) are more than the calculated P═S bond lengths in the related free ligands (L_1: 1.928 Å and L_2: 1.9285 Å). A decrease of the calculated P–N bond lengths in **1** (1.6536 Å), **2** (1.6394 and 1.6576 Å) and **3** (1.6459 Å) compared to those in L_1 (1.6779 Å) and L_2 (1.6761 Å) is also observed.

NBO analysis

The NBO method supports the orbital details, the possible percentage of the electron density, donor–acceptor interaction energy and delocalization of electron density between the occupied Lewis-type orbitals and the formally unoccupied non-Lewis orbitals through the second-order perturbation analysis by the Fock matrix. According to this procedure, the strengths of Hg–S and Hg–X bonds (X = Cl and Br) in **1**, **2** and **3** were estimated, with the calculation of second-order perturbation energies, $E^{(2)}$, for electronic delocalization from the main donor orbitals σ(P═S) and Lp(Cl or Br) to Lp*(Hg). Furthermore, the strengths of non-covalent interactions were evaluated by considering the electron delocalization from Lp(S, Cl, Br or O) or π-bonding orbital to the corresponding σ*(C–H or N–H). Natural atomic charges of the atoms participating in covalent bond and non-covalent bond interactions are listed in Table 2.

During the coordination of ligand to metal, the negative charge of the S atom increases and the calculated natural charges of S atoms are −0.61 for **1**, −0.58 and −0.63 for **2**, −0.62 and −0.57 for **3**, compared with −0.57 for both S atoms of L_1 and L_2. The positive charges of Hg atoms in complexes **1** (1.03) and **3** (1.00), including chloride, are greater than the positive charge of Hg in **2** (0.87) with bromide.

The stabilization energies, $E^{(2)}$, for σ(P═S) to Lp*(Hg) delocalizations were calculated as 4.57 and 3.59 kcal mol^{-1} for **1**, 5.71 and 4.89 kcal mol^{-1} for **2** and 3.98 and 2.03 kcal mol^{-1} for **3**. For both **1** and **3**, two $E^{(2)}$ for Hg–Cl^{t} and two $E^{(2)}$ for Hg–Cl^{b} (t = terminal, b = bridge) were calculated. In both complexes, the two Hg–Cl^{b} are stronger than the two Hg–Cl^{t} (for **1**, $E^{(2)}$(Hg–Cl^{b}): 24.40, 18.08 kcal mol^{-1} and $E^{(2)}$(Hg–Cl^{t}): 11.12, 9.83 kcal mol^{-1}; for **3**, $E^{(2)}$(Hg–Cl^{b}): 27.89, 20.12 kcal mol^{-1} and $E^{(2)}$(Hg–Cl^{t}): 15.35, 12.47 kcal mol^{-1}) (Table 2). The two stabilizing energies $E^{(2)}$ of Hg–Br in **2** are lower than the $E^{(2)}$ values of Hg–Cl in **1** and **3**.

As was reported in the structure description, the intermolecular interactions are as follows: N–H···Cl in **1**, three C–H···Br in **2**, C–H···Cl, and C–H···S in **3**. The calculated energies ($E^{(2)}$) of these interactions are given in Table 2. For the calculation of energies, the charge transfer interactions were considered from the donor orbital (Lp of Cl, Br or S, and π(C–C)) to the antibonding orbital of the acceptor (σ* of N–H or C–H).

Table 2 NBO parameters at the M06-2X/6-311++G(d,p)/LANL2DZ level

Complex	Donor orbital	Acceptor orbital	Natural charge: Donor (Cl, Br, O, S, π)	Natural charge: Acceptor (N–H, C–H, Hg)	$E^{(2)}$ (kcal mol^{-1})
1					
Hg–S	σ(P=S)	Lp*(Hg)	−0.61	1.05	4.57, 3.59
Hg–Cl^t	Lp(Cl)	Lp*(Hg)	−0.63, −0.65	1.03	11.12, 9.83
Hg–Cl^b	Lp(Cl)	Lp*(Hg)	−0.61	1.03	24.40, 18.08
N1–H1···Cl1	Lp(Cl)	σ*(N–H)	−0.64	0.32	2.66
C2–H2···O1	Lp(O)	σ*(C–H)	−0.89	0.23	2.59
C4–H4*A*···Cl1	Lp(Cl)	σ*(C–H)	−0.62	0.26	0.53
C7–H7*B*···Cg	π(C–C)	σ*(C–H)	−0.62	0.22	0.12
2					
Hg–S	σ(P=S)	Lp*(Hg)	−0.58, −0.63	0.87	5.71, 4.89
Hg–Br	Lp(Br)	Lp*(Hg)	−0.62, −0.57	0.87	8.44, 9.44
N1–H1···Br2	Lp(Br)	σ*(N–H)	−0.59	0.47	3.41
C4–H4*A*···Br2	Lp(Br)	σ*(C–H)	−0.59	0.23	0.63
C13–H13*B*···Br1	Lp(Br)	σ*(C–H)	−0.58	0.20	1.12
C10–H10···Br1	Lp(Br)	σ*(C–H)	−0.58	0.24	0.42
C4–H4*B*···S1	Lp(S)	σ*(C–H)	−0.60	0.23	0.52
C11–H11*B*···S2	Lp(S)	σ*(C–H)	−0.59	0.24	0.11
C9–H9···O4	Lp(O)	σ*(C–H)	−0.88	0.21	4.74
C3–H3···O2	Lp(O)	σ*(C–H)	−0.89	0.20	5.98
C14–H14*A*···Cg	π(C–C)	σ*(C–H)	−0.61	0.23	0.29
C14–H14*B*···Cg	π(C–C)	σ*(C–H)	−0.61	0.23	0.06
3					
Hg–S	σ(P=S)	Lp*(Hg)	−0.62, −0.57	1.05	3.98, 2.03
Hg–Cl^t	Lp(Cl)	Lp*(Hg)	−0.63, −0.64	1.00	15.35, 12.47
Hg–Cl^b	Lp(Cl)	Lp*(Hg)	−0.62	1.00	27.89, 20.12
C4–H4*C*···Cl1	Lp(Cl)	σ*(C–H)	−0.64	0.21	1.21
C5–H5*A*···Cl1	Lp(Cl)	σ*(C–H)	−0.65	0.20	0.95
C4–H4*A*···S1	Lp(S)	σ*(C–H)	−0.61	0.23	1.12

All of these interactions are weak and the most important calculated intermolecular interaction is N–H···Cl with $E^{(2)}$ = 2.66 kcal mol^{-1}. The intramolecular interactions in these structures are C–H···O, C–H···Cl and C–H···π in **1**, N–H···Br, C–H···O, C–H···S and C–H···π in **2** and C–H···Cl in **3**, with the highest calculated energy value of 5.98 kcal mol^{-1} for C–H···O (**2**).

For intermolecular interactions received by Cl atoms, the computed q(Cl) and q(H) for N–H···Cl in **1** are −0.64 and 0.32, respectively, typically compared with the values related to a weaker interaction C–H···Cl in **3** ($E^{(2)}$ = 1.21 kcal mol^{-1}, q(Cl) = −0.64 and q(H) = 0.21). For the intramolecular N–H···Br interaction in **2**, the computed q(Br) and q(H) are −0.59 and 0.47, respectively.

Topological analysis

In Quantum Theory of Atoms In Molecules (QTAIM) analysis, the strength and characteristic of a bond are investigated by the electron density $\rho(r)$ and its Laplacian $\nabla^2\rho(r)$, potential energy density $V(r)$, kinetic energy density $G(r)$, ratio of the potential energy density to the kinetic energy density $|V(r)|/G(r)$ and electronic energy density $H(r)$ ($H(r) = G(r) + V(r)$) at the BCP.[52] The high values of $\rho(r)$, $\nabla^2\rho(r) < 0$ and $H(r) < 0$ refer to the shared interaction or covalent bond, while the small values of $\rho(r)$, $\nabla^2\rho(r) > 0$ and $H(r) > 0$ denote the closed-shell interactions such as ionic bond, hydrogen bond and van der Waals interactions. The values of $\nabla^2\rho(r) > 0$ and $H(r) < 0$ assign intermediate interactions.[53] The sign of $\nabla^2\rho$ at a BCP is determined based on the equation $(1/4)\nabla^2(r) = 2G(r) + V(r)$. Thus, the magnitude of $H(r)$ at a BCP, instead of $\nabla^2\rho(r)$, might be a more reliable index for characterizing a weak interaction. Espinosa *et al.* have suggested that closed-shell, intermediate and shared interactions are associated with $|V(r)|/G(r) \leq 1$, $1 < |V(r)|/G(r) < 2$, and $|V(r)|/G(r) > 2$ ratios, respectively.[54]

The results of the topological analysis at the BCPs of Hg–S and Hg–X (X = Cl and Br) covalent bonds and different hydrogen bonds observed in structures **1**, **2** and **3** are summarized in Table S3.† For **1**, the electron density values of 0.67/0.67, 0.63/0.64 and 0.57/0.57 a.u. were estimated at the BCPs of 2 × Hg–S, 2 × Hg–Cl^t, and 2 × Hg–Cl^b, respectively. Based on the ρ values, $\nabla^2\rho(r) > 0$ and $H(r) < 0$, the Hg–S, Hg–Cl^t and Hg–Cl^b bonds show medium-strength with a mainly electrostatic nature and a partial covalent character. For these bonds, the $|V(r)|/G(r)$ values of 1.30/1.30, 1.18/1.18 and 1.15/1.15 a.u. confirm their intermediate nature with the dominance of the ionic character.

Similarly for Hg–S and Hg–X (X = Cl and Br) covalent bonds in both **2** and **3**, the ρ values are small and the corresponding $\nabla^2\rho$ values are positive and the $H(r)$ values are negative, which show a principally electrostatic nature with a partial covalent contribution.

A comparison of Hg-halide bonds in **1** and **2** (with the equal L_1 ligand) shows lower ρ values at the two Hg–Br BCPs with respect to the ones at the Hg–Cl^t BCPs. The $|V(r)|/G(r)$ ratios for Hg–Br bonds at BCPs (1.50 and 1.46 a.u.) also confirm their intermediate nature with a contribution of the ionic character (Table S3†).

A comparison of **1** and **3** with a similar inorganic fragment but with different spacers, *i.e.* [1,4-(NH)$_2$C$_6$H$_4$] in **1** and [1,4-(N)$_2$C$_4$H$_8$] in **3** shows higher ρ values at the Hg–Cl^b BCPs and smaller ρ values at the Hg–Cl^t BCPs for **1**. In addition, the values of the $|V(r)|/G(r)$ ratio for Hg–Cl^t in **3** are greater, and those of Hg–Cl^b are smaller than the ones in **1**.

For the intermolecular interactions, the $\rho(r)$ values are within 0.12–0.96 a.u. and the corresponding $\nabla^2\rho(r)$ and $H(r)$ values are positive for all, showing their electrostatic nature (Table S3†). Similar results were observed for the intramolecular interactions, with the $\rho(r)$ values in the range of 0.10–0.85 a.u.

Hirshfeld surface analysis

For a detailed description of interactions involved in crystal packing, it was decided to use Hirshfeld surface (HS) analysis including fingerprint (FP) plot. In the Hirshfeld surface maps (mapped with d_{norm}), the contacts shown in red highlight the interactions with distances closer than the sum of the van der Waals radii, while white is used for the contacts around the vdW separation, and blue represents longer contacts.[42]

The three-dimensional HSs, mapped with d_{norm}, were generated for **1**, **2** and **3** (around the Hg_2Cl_4L fragment for **1** and **3**, L = L_1 (**1**) and L_2 (**3**), and around $HgBr_2L_1$ for **2**), as shown in Fig. 5. In complex **2**, there are two-half independent thiopho-

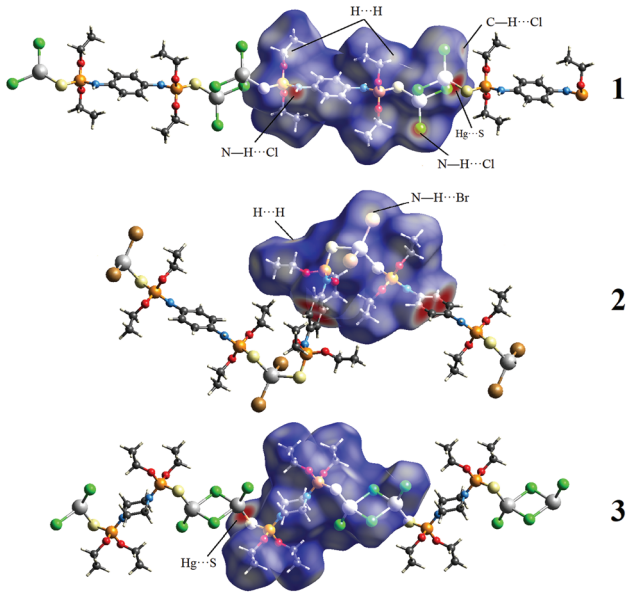

Fig. 5 The Hirshfeld surfaces mapped with d_{norm} for visualizing some important interactions in structures **1**, **2** and **3**.

sphoramide ligands in the structure and the fragment $HgBr_2L_1$ is indeed $HgBr_2(L_1)_{0.5}(L_1)_{0.5}$ which was used for the construction of Hirshfeld surface maps.

In the HS map of **1**, the large red regions are related to the Hg···S bond and N–H···Cl hydrogen bond, and one light red region and two very light red areas are related to the C–H···Cl and H···H contacts. For **2**, the N–H···Br hydrogen bond and H···H contact are highlighted, however, there are also very large red areas in the HS map related to the C–C bonds (as the HS map was generated around one-half of each thiophosphoramide ligand coordinated to Hg).

The N–H···Br hydrogen bond noted was observed between adjacent N–H and Br within a chain. The darker red color for the H···H contact in **2** with respect to a similar contact in **1** shows a closer contact. In both these structures, the H···H contacts occurred between the ethyl groups.

In **3**, the Hirshfeld surface reveals one red area, associated with the Hg···S bond, and the contacts involving hydrogen atoms within a coordination polymer and/or between adjacent coordination polymeric chains are not highlighted in this structure.

The contribution percentages of different contacts in the crystals of **1**, **2** and **3** are shown in Fig. 6, and typically the

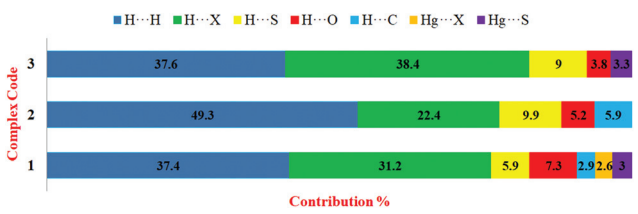

Fig. 6 Percentage contributions of contacts to the Hirshfeld surface in the structures calculated from the crystal structures of **1**, **2** and **3**.

divided fingerprint plots of **1** are given in Fig. 7, while the ones for **2** and **3** are given in Fig. S8 and S9 in the ESI,† respectively.

It is evident that in all three complexes, the H···H contacts are predominant, with contributions of 37.4, 49.3 and 37.6% for **1**, **2** and **3**, respectively. The second most significant interaction is H···X, X = Cl (**1** and **3**) and Br (**2**), with contributions of 31.2% (**1**), 22.4% (**2**) and 38.4% (**3**). Structures **1** and **2** include C···H contacts due to the presence of unsaturated C atoms involved in H···π interactions as discussed in the X-ray description.

Spectroscopy investigations

IR spectroscopy. The P═S stretching band of L_1 was reported at 729 cm^{-1} in the literature,[27] and the band assigned to P═S in complex **2** shows no shift with respect to the free ligand and in complex **1** the corresponding band is very weak (at 727 cm^{-1}). The reason for equal P═S stretching frequencies is attributed to the presence of the H···S═P interaction in L_1 which replaces Hg···S═P in the complexes. Similar observations were reported for some P═O containing compounds involving hydrogen bonding and the related metal complexes.[55] Similar bands in **3**/L_2 show a more significant difference in the frequencies and appear at 702/714 cm^{-1}.

NMR spectroscopy. The signals of L_1, L_2, **1** and **3** appear in the expected regions of chemical shifts. The $^{31}P\{^1H\}$ signals appear at 65.42/65.09 ppm for L_1/**1** (both in CD_3CN) and at 73.64/73.34 ppm for L_2/**3** (both in DMSO-d_6). The methyl and methylene protons of complexes **1** and **3** show the triplet and multiplet (doublet of quartets) fine structures. In the ^{1}H-NMR of L_1/**1**, the doublet signals appear for NH units at 6.21/6.28 ppm ($^2J_{P-H}$ = 14.4/14.4 Hz) and the ^1H–^{15}N HSQC spectra show cross-peaks at {−294.93, 6.23 ppm} for L_1 and at {−298.20, 6.25 ppm} for **1**. The methyl carbon signals appear as doublets at 15.12/16.12 ppm ($^3J_{P-C}$ = 8.2/8.1 Hz) for L_1/L_2 and as doublets at 15.09/16.14 ppm ($^3J_{P-C}$ = 8.3/10.7 Hz) for **1**/**3**. The doublets at 62.90 ppm ($^2J_{P-C}$ = 4.5 Hz) for L_1 and at 62.87 ppm ($^2J_{P-C}$ = 5.3 Hz) for L_2 are related to the CH_2 of the ethyl group. Similar signals in the related complexes appear as doublets, at 63.12 ppm in complex **1** ($^2J_{P-C}$ = 4.7 Hz) and 63.01 ppm in complex **3** ($^2J_{P-C}$ = 7.4 Hz). The CH_2 group of the $N_2C_4H_8$ linker in L_2 and complex **3** appears as doublets at 45.33 ppm ($^2J_{P-C}$ = 8.1 Hz) and at 45.30 ppm ($^2J_{P-C}$ = 9.4 Hz), respectively. The differences between coupling constants are more significant in the case of **3**/L_2 with respect to those in **1**/L_1. The presence of one phosphorus signal in the solution study of complexes **1** and **3** suggests that the data are associated with the $Cl_2Hg(\mu\text{-}L)HgCl_2$ monomers (L = L_1 and L_2) in solution, as more than one phosphorus signal is expectable for a polymeric structure. The cleavage of the polymeric structure should have occurred at the position of the weaker Hg–Cl[b] bond (as was noted in the X-ray crystallography section). Complex **2** was insoluble in NMR solvents. $^{31}P\{^1H\}$, ^1H, ^{13}C NMR, ^1H–^{15}N HSQC for L_1, L_2, **1** and **3** are represented in Fig. S10–S23 in the ESI.†

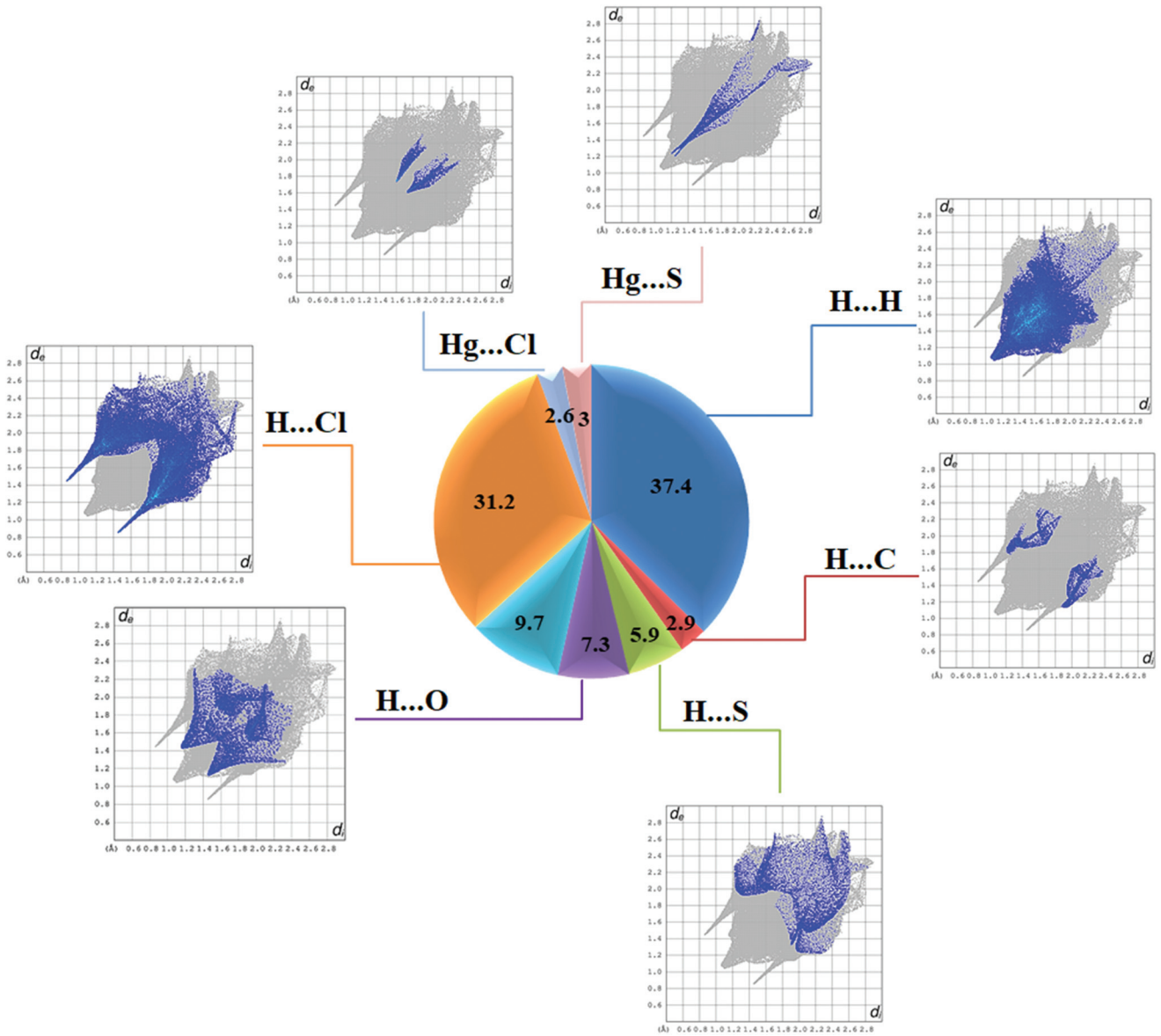

Fig. 7 Schematic illustration of the fingerprint plots of **1**. Different colors have been used for different atom pair contacts.

Mass spectrometry. The mass spectra of complexes **1**, **2** and **3** were recorded in both 20 and 70 eV conditions. For **1**, the peak at m/z = 684 in the 20 eV experiment is assigned to the $^{35}Cl_2{}^{202}HgL_1$ cation, but the appearance of a peak at m/z = 751 is surprising and is in accordance with one-half of the $Hg_2Cl_4L_1Hg_2Cl_4$ (^{202}Hg, 6 × ^{35}Cl and 2 × ^{37}Cl) cationic fragment. In the 70 eV experiment, the peak at 648 is assigned to the $[^{35}Cl_2{}^{202}HgL_1–H^{35}Cl]$ cation. For **2**, the peak at m/z = 772, assigned to the $^{79}Br_2{}^{202}HgL_1$ molecular ion peak, is observed in both 20 and 70 eV conditions at a low intensity (a few more in 20 eV), and the peak at m/z = 412 (L_1^+) is important in both experiments (base peak in 20 eV). For **3**, low intense fragments 662 in 20 eV and 663 in 70 eV are assigned to the $[^{35}Cl_2{}^{202}HgL_2]^+$ and $[^{35}Cl_2{}^{202}HgL_2 + 1]^+$, respectively and the base peak appears at m/z = 169 ($[C_4H_{12}NO_2PS]^+$) in both mass experiments. The base peaks for **1** (in both experiments) and for **2** (in 70 eV) are related to low weight cationic fragments, as assigned in the Experimental section. For each of the three complexes, the peak related to the mercury-halide is seen. It should be noted that the seven isotopes ^{198}Hg to ^{204}Hg can be seen in the mass spectra of mercury-containing compounds. Thus, the cationic fragments including mercury usually appear as a set of neighbor peaks. Mass spectra are presented in Fig. S24–S29 in the ESI.†

Conclusions

A survey of the Cambridge Structural Database shows 1482 structures with Hg–S bonds and in this work, we present the

first examples of mercury complexes with $[O]_2[N]P(S)$-based ligands. The complexes are one dimensional coordination polymers $\{Hg_2Cl_4L_1\}_n$ (**1**), $\{HgBr_2L_1\}_n$ (**2**) and $\{Hg_2Cl_4L_2\}_n$ (**3**), [L_1 = $(EtO)_2P(S)(NHC_6H_4NH)P(S)(OEt)_2$ and L_2 = $(EtO)_2P(S)(NC_4H_8N)P(S)(OEt)_2$]. The mercury atoms in all three complexes adopt an almost trigonal pyramidal shape, $HgCl_3S$ for **1**/**3** and $HgBr_2S_2$ for **2**, and the Hg–S bond in the three complexes and the Hg–Cl bond formed by the bridging chlorine in **1** and **3** are responsible for the construction of the polymeric structure. The difference observed in the stoichiometry of metal to the thiophosphoramide ligand in **1** and **3** with respect to that in **2** is a result of the contribution of bridging chlorido ligands in the formation of the Hg_2Cl_2 ring, however, the molar ratio 2 : 1 of HgX_2 (X = Cl and Br) to ligand was used for the preparation of all three complexes. The chlorine-containing complexes are soluble in some solvents, such as CH_3CN, and the bromine-containing complex is insoluble in some solvents examined, and the solution NMR experiments were performed for **1** and **3** in CD_3CN and DMSO-d_6, respectively. The supramolecular architectures formed by N–H···Cl in **1**, C–H···Br in **2** and C–H···S/C–H···Cl in **3** were discussed. The energies of Hg–Cl, Hg–Br and Hg–S as well as the interactions building supramolecular assemblies, and intramolecular interactions, *i.e.* NH···Cl, NH···Br, CH···Cl, CH···Br, CH···O, CH···S, and CH···π, were theoretically evaluated. The coordination polymers constructed with the $[O]_2[N]P(S)$-based ligands may be extended to the synthesis of two-dimensional and three-dimensional coordination polymers using new designed ligands containing more than two P═S groups and/or including both P═S and other coordinating groups. The flexibility and volume of linkers attached to the P═S groups may be changed in order to design new potential ligands. It is also possible to study (CSD survey combined with new experimental/theoretical data) the difference in the strengths of $Hg–Cl^b$ (b = bridge) in the Hg_2Cl_2 rings which may be one of the factors influencing the solubility of Hg_2Cl_4-containing compounds.

Conflicts of interest

There are no conflicts to declare.

Acknowledgements

Support for this investigation by the Ferdowsi University of Mashhad is gratefully acknowledged (project 3/33548). We thank the Russian Foundation for Basic Research (project 16-33-00942) and the Ministry of Education and Science of The Russian Federation (project 4.619.2014/K). The authors appreciatively acknowledge the Cambridge Crystallographic Data Centre for access to the CSD Enterprise.

Notes and references

1 B. Moulton and M. J. Zaworotko, *Chem. Rev.*, 2001, **101**, 1629.
2 S. R. Batten, S. M. Neville and D. R. Turner, *Coordination polymers: design, analysis and application*, Royal Society of Chemistry, 2008.
3 P. G. Derakhshandeh, J. Soleimannejad, J. Janczak, A. M. Kaczmarek, K. V. Hecke and R. V. Deun, *CrystEngComm*, 2016, **18**, 6738.
4 A. M. Ako, C. S. Hawes, B. Twamley and W. Schmitt, *CrystEngComm*, 2017, **19**, 994.
5 W. L. Leong and J. J. Vittal, *Chem. Rev.*, 2011, **111**, 688.
6 M. J. Plater, M. R. St. J. Foreman, T. Gelbrich, S. J. Coles and M. B. Hursthouse, *J. Chem. Soc., Dalton Trans.*, 2000, 3065.
7 C. Janiak, *Dalton Trans.*, 2003, 2781.
8 M. Barceló-Oliver, B. A. Baquero, A. Bauzá, Á. García-Raso, R. Vich, I. Mata, E. Molins, À. Terrón and A. Frontera, *Dalton Trans.*, 2013, **42**, 7631.
9 A. Saneei, M. Pourayoubi, A. Crochet and K. M. Fromm, *Acta Crystallogr., Sect. C: Struct. Chem.*, 2016, **72**, 230.
10 C. Hu, I. Kalf and U. Englert, *CrystEngComm*, 2007, **9**, 603.
11 D. C. Bebout, M. M. Garland, G. S. Murphy, E. V. Bowers, C. J. Abelt and R. J. Butcher, *Dalton Trans.*, 2003, 2578.
12 D. B. Tice, R. D. Pike and D. C. Bebout, *Dalton Trans.*, 2016, **45**, 12871.
13 N. J. Williams, R. D. Hancock, J. H. Riebenspies, M. Fernandes and A. S. de Sousa, *Inorg. Chem.*, 2009, **48**, 11724.
14 I. G. Dance, *Polyhedron*, 1986, **5**, 1037.
15 K. M. Rice, E. M. Walker Jr., M. Wu, C. Gillette and E. R. Blough, *J. Prev. Med. Public Health*, 2014, **47**, 74.
16 E. Bermejo, A. Castiñeiras, I. García-Santos and R. Rodríguez-Riobó, *CrystEngComm*, 2016, **18**, 3428.
17 M. Taş, M. Yağan, H. Batı, B. Batı and O. Büyükgüngör, *Phosphorus, Sulfur Silicon Relat. Elem.*, 2010, **185**, 242.
18 C. R. Groom, I. J. Bruno, M. P. Lightfoot and S. C. Ward, *Acta Crystallogr., Sect. B: Struct. Sci., Cryst. Eng. Mater.*, 2016, **72**, 171.
19 V. Cadierno, P. Crochet, J. Díez, J. García-Álvarez, S. E. García-Garrido, S. García-Granda, J. Gimeno and M. A. Rodríguez, *Dalton Trans.*, 2003, 3240.
20 D. A. Safin, M. G. Babashkina, M. Bolte, T. Pape, F. E. Hahn, M. L. Verizhnikov, A. R. Bashirov and A. Klein, *Dalton Trans.*, 2010, **39**, 11577.
21 M. G. Babashkina, D. A. Safin, A. P. Railliet, M. Bolte, A. Brzuszkiewicz, H. Kozlowski and Y. Garcia, *New J. Chem.*, 2012, **36**, 2642.
22 D. A. Safin, M. G. Babashkina and Y. Garcia, *Dalton Trans.*, 2013, **42**, 902.
23 Y. Zhou, M. Hong and X. Wu, *Chem. Commun.*, 2006, 135.
24 D. A. Safin, M. G. Babashkina, P. Kubisiak, M. P. Mitoraj, K. Robeyns, E. Goovaerts and Y. Garcia, *Dalton Trans.*, 2013, **42**, 5252.
25 F. D. Sokolov, M. G. Babashkina, F. Fayon, A. I. Rakhmatullin, D. A. Safin, T. Pape and F. E. Hahn, *J. Organomet. Chem.*, 2009, **694**, 167.
26 V. Cadierno, J. Díez, J. García-Álvarez and J. Gimeno, *Dalton Trans.*, 2007, 2760.
27 Y. Ren, B. Cheng, J. Zhang, H. Zang, W. Kang and C. Ding, *Front. Chem. China*, 2008, **3**, 304.

28 Agilent, *CrysAlis PRO*, Agilent Technologies Ltd, Yarnton, Oxfordshire, England, 2014.
29 G. M. Sheldrick, *Acta Crystallogr., Sect. C: Struct. Chem.*, 2015, **71**, 3.
30 G. M. Sheldrick, *Acta Crystallogr., Sect. A: Found. Adv.*, 2015, **71**, 3.
31 O. V. Dolomanov, L. J. Bourhis, R. J. Gildea, J. A. K. Howard and H. Puschmann, *J. Appl. Crystallogr.*, 2009, **42**, 339.
32 M. Frisch, G. Trucks, H. Schlegel, G. Scuseria, M. Robb, J. Cheeseman, G. Scalmani, V. Barone, B. Mennucci and G. Petersson, *GAUSSIAN09*, Gaussian Inc., Wallingford, CT, USA, 2009.
33 Y. Zhao and D. G. Truhlar, *Theor. Chem. Acc.*, 2008, **120**, 215.
34 P. J. Hay and W. R. Wadt, *J. Chem. Phys.*, 1985, **82**, 299.
35 E. Glendening, A. Reed, J. Carpenter and F. Weinhold, *NBO, Version 3.1*, Gaussian Inc., Pittsburgh, PA, 2003.
36 R. Bader, *In Atoms in Molecules. A Quantum Theory*, Oxford University Press Inc., New York, 1998.
37 T. Lu and F. Chen, *J. Comput. Chem.*, 2012, **33**, 580.
38 M. A. Spackman and D. Jayatilaka, *CrystEngComm*, 2009, **11**, 19.
39 J. J. McKinnon, D. Jayatilaka and M. A. Spackman, *Chem. Commun.*, 2007, 3814.
40 J. K. Zaręba, M. J. Białek, J. Janczak, J. Zoń and A. Dobosz, *Cryst. Growth Des.*, 2014, **14**, 6143.
41 A. Pietrzak, J. Modranka, J. Wojciechowski, T. Janecki and W. M. Wolf, *Cryst. Growth Des.*, 2018, **18**, 200.
42 S. Wolff, D. Grimwood, J. McKinnon, M. Turner, D. Jayatilaka and M. Spackman, *Crystal Explorer 3.1*, University of Western Australia, Crawley, Western Australia, 2013.
43 L. K. Rana, S. Sharma and G. Hundal, *Cryst. Growth Des.*, 2016, **16**, 92.
44 G. Mahmoudi and A. Morsali, *CrystEngComm*, 2009, **11**, 1868.
45 F. H. Herbstein, P. Ashkenazi, M. Kaftory, M. Kapon, G. M. Reisner and D. Ginsburg, *Acta Crystallogr., Sect. B: Struct. Sci.*, 1986, **42**, 575.
46 J. Dai, M. Munakata, G.-Q. Bian, Q.-F, Xu, T. Kuroda-Sowa and M. Maekawa, *Polyhedron*, 1998, **17**, 2267.
47 W. Lu, P. S. Barber, S. P. Kelley and R. D. Rogers, *Dalton Trans.*, 2013, **42**, 12908.
48 X. Zhang, Y. Xie, W. Yu, Q. Zhao, M. Jiang and Y. Tian, *Inorg. Chem.*, 2003, **42**, 3734.
49 X.-Y. Tang, J.-X. Chen, G.-F. Liu, Z.-G. Ren, Y. Zhang and J.-P. Lang, *Eur. J. Inorg. Chem.*, 2008, **2008**, 2593.
50 M. Taherzadeh, M. Pourayoubi and M. Nečas, *Phosphorus, Sulfur Silicon Relat. Elem.*, 2019, **194**, 39.
51 L. Yang, D. R. Powell and R. P. Houser, *Dalton Trans.*, 2007, 955.
52 R. F. W. Bader, *Chem. Rev.*, 1991, **91**, 893.
53 W. Koch, G. Frenking, J. Gauss, D. Cremer and J. R. Collins, *J. Am. Chem. Soc.*, 1987, **109**, 5917.
54 E. Espinosa, I. Alkorta, J. Elguero and E. Molins, *J. Chem. Phys.*, 2002, **117**, 5529.
55 M. Pourayoubi, M. Toghraee, R. J. Butcher and V. Divjakovic, *Struct. Chem.*, 2013, **24**, 1135.